SOCIETY FOR SCIENCE AND EDUCATION UNITED KINGDOM

JBEMi JOURNAL OF BIOMEDICAL ENGINEERING AND MEDICAL IMAGING

ISSN: 2055-1266
VOLUME 3 ISSUE 6

Development of Contactless Cauterization Device for Surgery Using A Steam-Jet

[1]Hitoshi Yoshiki, [2]Kotaro Tadano, [3]Daisuke Ban, [4]Katsuhiro Ohuchi, [3]Minoru Tanabe, and [5]Kenji Kawashima

[1]Department of Mechano-Micro Engineering, Tokyo Institute of Technology, Japan;
[2] Laboratory for Future Interdisciplinary Research of Science and Technology, Tokyo Institute of Technology, Japan;
[3] Department of Hepatobiliary-Pancreatic Surgery, Tokyo Medical and Dental University, Japan
[4] Department of Advanced Surgical Technology Research and Development, Tokyo Medical and Dental University, Japan
[5] Department of Biomechanics, Tokyo Medical and Dental University, Japan
yoshiki.h.aa@m.titech.ac.jp

ABSTRACT

To improve outcomes in surgery, surgical energy devices which perform coagulation and cauterization with shorter operating time, less thermal injury, and less adherence are required. In this paper, basic principles and cauterization mechanisms of cauterization method with steam-jet were studied. The steam-jet coagulator (SJC) was newly developed with dry-steam generator for effective heat-transfer with steam. The condensation heat-transfer coefficient at the surface was estimated through thermofluidic simulations and experimental temperature distributions inside the heated object by impinging steam-jet. The steam-jet of 10kPa(G) and 30kPa(G) were estimated to have the heat-transfer coefficients larger than 5.0×10^5 W/m^2 under several design parameters. Histological images of coagulated hepatic tissues with the SJC, the bipolar electrocautery device, and the bipolar with the saline irrigation method were compared. The comparison revealed that steam-jet can coagulate tissue denser and can seal sinusoids better than the ones coagulated with the bipolar electrocautery device even if the saline irrigation method was used. Successful coagulation and cauterization were performed on the *in-vivo* experiment using porcine liver, and thus the feasibility of the proposed method was confirmed. Our findings represent the engineering principles, the histological mechanisms, and the feasibility in *in-vivo* situations of the contactless cauterization device using a steam-jet.

Keywords: Coagulation; Compressible flow; Condensation heat transfer, In-vivo experiment; Prototype; Surgical instruments; Steam jet

1 Introduction

Surgical energy devices are essential tools for modern medical treatments. These devices apply electricity, mechanical vibration, heat, lasers, or other forms of energy to biological tissue to cut it, coagulate it, or lead it to cell death. Several methods in modern surgery highly depend on the surgical

DOI: 10.14738/jbemi.36.2335
Publication Date: 23rd November 2016
URL: http://dx.doi.org/10.14738/jbemi. 36.2335

energy devices; thus, the development of surgical devices is important for further improvement in surgeries [1-2].

Conventional devices have three challenges: a trade-off between effectiveness and minimal-invasiveness, avoidance of unintended overheating, and removal of adhering substances. Surgical outcomes are assessed with several parameters such as operative time, rates of injury, volume of blood loss, and mortality rate [3-4]. To improve the outcome, quick and effective device contributes much for operative time reduction. However, coagulation requires much operating time and low output power with conventional devices because these devices with high output power causes a tissue carbonization and larger thermal injury [5-6]. Adherence of biological substances such as fat, blood, and mucosa is hindering the applied energy by the surgical energy devices. Removal of the tissue requires interruption of a surgical procedures.

To improve outcomes of surgeries, we aim to develop a surgical energy device that can perform coagulation with shorter operating time, less thermal injury, and adherence of tissue. We have preliminarily proposed a new type of surgical energy device using a steam jet for faster cauterization without adherence of tissues [7]. In the previous report we described the basic concept of steam-jet coagulation and confirmed its characteristics with a simple prototype. The scope of this report was rather limited because of the lack of a thermofluidic analysis for further design and a dry steam generation mechanism for shorter coagulation time with larger heat-transfer coefficient. In addition, the mechanism of coagulation was not studied with histological perspective.

In this paper, the authors describe basic principles and cauterization mechanisms of the steam-jet coagulator (SJC) we proposed and developed. The condensation heat-transfer coefficients of steam-jet were estimated through the comparison between thermofluidic analysis and experimental temperature distribution. Coagulation effects of SJC were studied through *ex vivo* histological comparison with the bipolar electrocautery device. The developed SJC performed cauterization successfully in *in vivo* experiments using a pig.

2 Materials and Methods

2.1 Prototype of Steam Jet Coagulator

The SJC was developed to perform coagulation and cauterization with dry steam. Moreover, it was designed with the ability to control pressure for experiments with several condition parameters. Figure 1 is a schematic diagram of the developed SJC. Steam flows from the steam-generator into the steam-buffer tank with a thermostatic steam trap. As steam flows in from the top of the steam-buffer, air, which has larger density, is gathered at the bottom. The steam trap ejects the air and drain water from the bottom of the tank, allowing dry steam to fill the tank. A reduction valve behind the tank controls the pressure of steam flow. A dry steam jet is released into an outlet of the nozzle section from the steam-control section.

Figure 2 shows the apparatus of the fabricated SJC. Four large wheels are fitted at the bottom of the apparatus so that it can be brought easily into an operating room. The top panel of the SJC is a control panel with switches and displays for manual control. The design is described in detail in the following sections. The boiler section of the SJC (shown in Figure 2(b)) consists of a boiler tank, a 1 kW electrical

heater, a sight tube, a safety valve, a pipe siphon, a pressure transducer, and a pressure indicator. The inner volume of the boiler tank is 9.0×10^5 mm^3. The tank is made of SUS304. The top and bottom plates of the tank are fastened with stainless bolts and sealed with exfoliated graphite gaskets so that the sealing withstands cyclic heating. Steam is generated from pure water with a 1 kW electrical heater in the boiler tank.

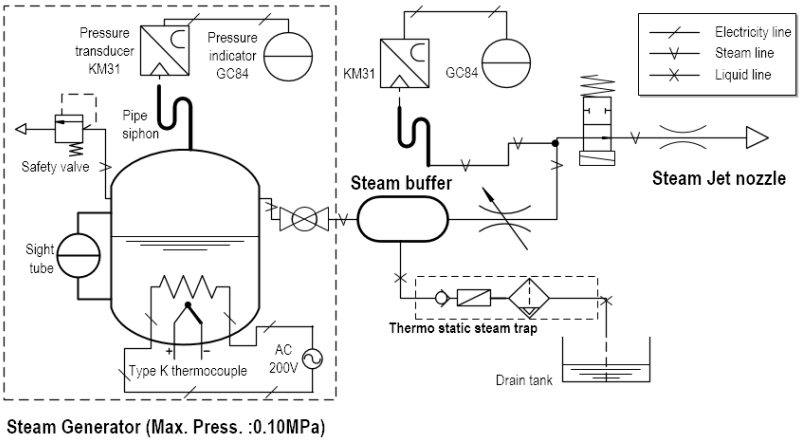

Figure 1. Schematic diagram of the prototype of the steam-jet coagulator

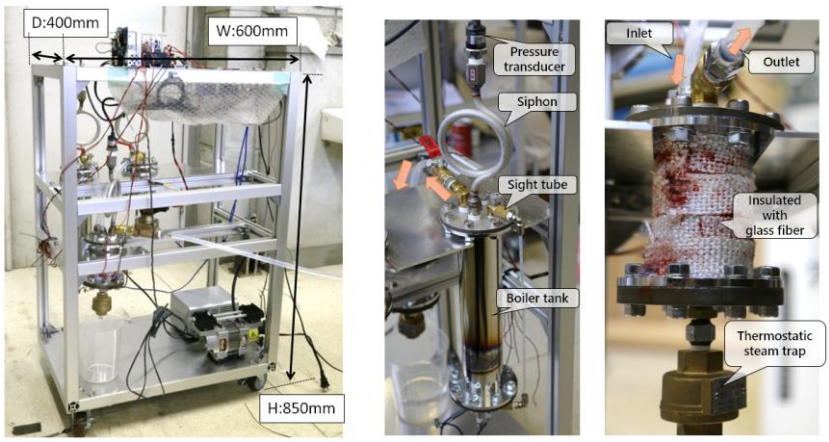

(a) Whole view (b) Steam generator (c) Steam buffer

Figure 2. Fabricated prototype of the steam-jet coagulator

The steam-jet nozzle (Figure3) was designed with considerations for handleability and sufficient insulation. The exterior package of the handle of the nozzle is made of polypropylenes (PP), which can be used continuously under 100ºC and are biocompatible. The package holds the nozzle core, which is made of polyetheretherketone (PEEK, TECAPEEK MT natural of Victrex plc.) inside with a small contact area, such that heat flux from the nozzle core to the exterior is limited. The nozzle tip is also made of PEEK. Three versions of nozzles with different outlet diameters (1.0 mm, 0.5 mm, 0.3 mm) are fabricated. Steam flows from the solenoid valve to the nozzle core via a silicone tube 10 mm in diameter. Then the steam passes through the core and flows out from the tip.

Figure 3. Apparatus of the nozzle for steam-jet application

2.2 Heat-Transfer Analysis

2.2.1 Definitions of Analysis Model

The nozzle was considered to be an orifice; thus, the flow speed of steam at the nozzle was derived by Eq. (1) and Eq. (2). Eq. (1) was for subsonic flow and Eq. (2) was for choked flow. The critical pressure ratio, *b,* was derived by Eq. (3). Steam's *b* is 0.5386.

Table 1 is the nomenclature for this thermofluidic analysis.

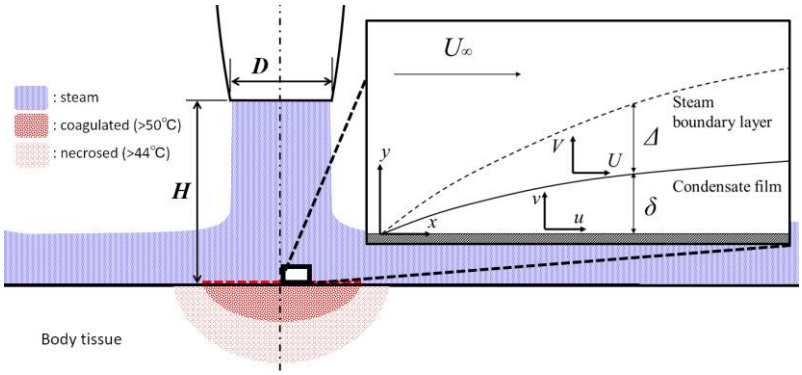

Figure 4. Model of impinging steam-jet for condensation heat-transfer analysis.

Table 1. Nomenclature for the heat-transfer analysis.

B	: Critical pressure ratio	Pr_L	: Prandtl number of liquid (water)
c_p	: Specific heat at constant pressure	Ph	: Phase change number as nondimensional parameter
D	: Diameter of hole of nozzle	u_{st}	: Flow speed of steam
d_{cd}	: Diameter of condensation area	R_{st}	: Individual gas constant of steam
H	: Height from object to nozzle	θ_{st}	: Temperature of steam
h_{th}	: Theoretical heat transfer coefficient	κ	: Heat capacity ratio of steam
h_f	: Experimental heat transfer coefficient	λ	: Thermal conductivity
l	: Representative length at the surface	$\mu_{L,V}$	: Static viscosity (L; liquid, V; vapor)
P_{st}	: Gauge pressure of steam	$\rho_{L,V}$	: Density (L; liquid, V; vapor)
P_{out}	: Gauge pressure of environmental atmosphere	ρ_{out}	: Density of environmental atmosphere
$P_{st\,(abs)}$	: Absolute pressure of steam		
$P_{out(abs)}$	: Absolute pressure of environmental atmosphere		

2.2.2 Theoretical Heat-Transfer Coefficient

To estimate the range of experimental heat-transfer coefficients, the authors derived theoretical heat-transfer coefficients. We applied forced convection film condensation theory over a horizontal plate to a fine region near the condensation surface of the analysis model with three assumptions: (1) the steam-boundary layer and condensate film are sufficiently thin due to the vertical force of the impinging jet; (2) the flow-speed vector of steam is parallel to the condensation surface due to continuity; and (3) the deceleration of steam flow can be neglected in the region. These assumptions are considered legitimate on account of the smallness of the target region (10^{-4}–10^{-2} m) and the magnitude of the flow speed (>10^2 m/s).

To confirm the applicability of the assumption on the flow speed of the steam-jet, we calculated the flow speed. In the calculation, the nozzle was considered to be an orifice; thus, the flow speed of steam at the nozzle is derived by Equation (1) and Equation (2). Equation (1) is for subsonic flow and Equation (2) is for choked flow. The critical pressure ratio b of steam is 0.5386.

$$u_{st} = \frac{P_{st(abs)}}{\rho_{out}} \sqrt{\left(\frac{2\kappa}{\kappa-1}\right) \cdot \frac{1}{R_{st}\theta_{st}} \left[\left(\frac{P_{out(abs)}}{P_{st(abs)}}\right)^{\frac{2}{\kappa}} - \left(\frac{P_{out(abs)}}{P_{st(abs)}}\right)^{\frac{\kappa+1}{\kappa}} \right]} \tag{1}$$

$$u_{st} = \frac{P_{st(abs)}}{\rho_{out}} \sqrt{\frac{\kappa}{R_{st}\theta_{st}} \left(\frac{2}{\kappa+1}\right)^{\frac{\kappa+1}{\kappa-1}}} \qquad \left(\frac{P_{out}}{P_{st}} \le b\right) \tag{2}$$

Note that the equation (2) for choke flows indicate that flow speed is independent of D and P_{out}. The SJC uses steam at saturated pressure; thus, θ_{st} is a function of P_{st}. Therefore, the flow speed of steam can be controlled by P_{st}, which is adjustable by the user. Figure 5 shows the theoretical flow speed of saturated steam. The physical properties of steam are referenced from the Steam Table of NIST [8]. The given density of steam differs at each calculated pressure; thus, calculation results are discrete. From the result of flow speed calculation (Figure5), steam-jet speed u_{st} assumed to be larger than 100 m/s when P_{st} is larger than at least 10kPa(G). Therefore, the three assumptions for forced convection film-wise condensation heat transfer theory can be applied.

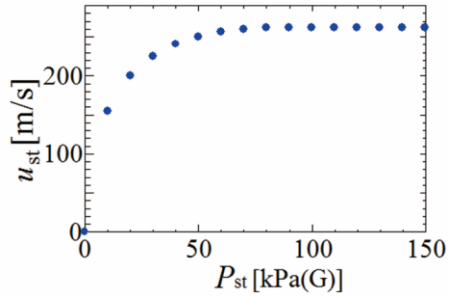

Figure 5. Calculated flow speed of steam-jet

The theoretical heat-transfer coefficient h_{th} at the condensation area from x=0 (the center of the area) to x=l is given by the theory for forced convection film condensation over a horizontal plate (Equation (4)).

$$Nu_l = 0.90(Re_l)_L^{1/3}(1.20+1/R\cdot Ph)^{1/3} \tag{4}$$

where

$$(Re_l)_L = u_{st} l/\nu_L \tag{5}$$

$$R\cdot Ph = (\rho_L \mu_L/\rho_V \mu_V)^{1/2}\cdot c_{pL}(T_{sat}-T_w)/Pr_L \tag{6}$$

2.2.3 Estimation of Experimental Heat-Transfer Conditions

Direct measurement of the heat-transfer coefficient was difficult because the estimated flow speed of the jet was too large. Hence, the authors measured the temperature distribution of an object that was exposed to the jet instead and used it to estimate the heat-transfer coefficient. The object used for the temperature distribution measurement is shown in Figure6.

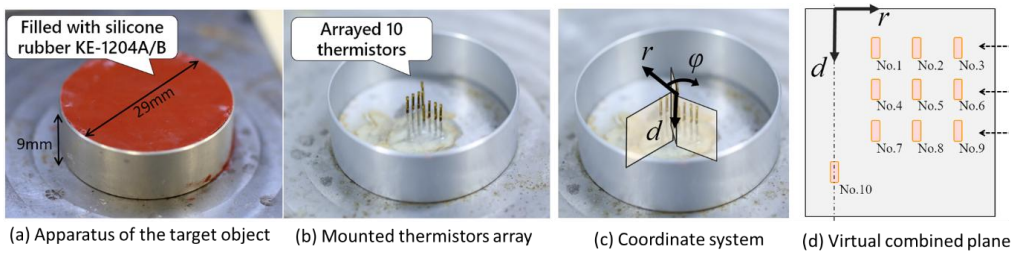

(a) Apparatus of the target object (b) Mounted thermistors array (c) Coordinate system (d) Virtual combined plane

Figure 6. Target object for experimental temperature distribution measurement

The simulation of temperature distributions in the object were conducted using assumed values of the heat-transfer coefficient at the condensation area, h_{th} and the diameter of the condensation area, d_{cd}. Figure 7 shows a cross-sectional simulation model of the heated object and the given boundary conditions of the simulation. The size of the model was equal to that of the object. Condensation heat-transfer areas of h_{th} and d_{cd} were set at the center of the top surface of the model, assuming that the steam jet was applied vertically to the center. The peripheral surface at the top was assumed to be exposed to the steam-jet flow and entrained air, and thus the heat-transfer coefficient at the peripheral surface was set to 200 W/m^2, which is a normal value for forced convection over a flat plate with air flow. The boundary conditions of other surfaces were assumed to have free convection with air.

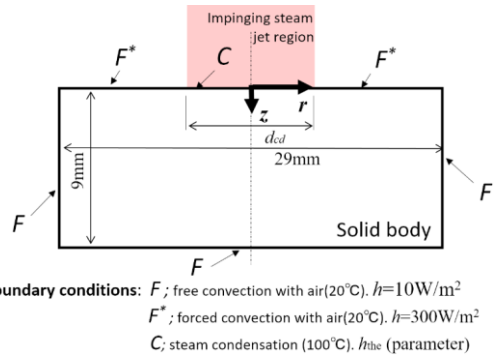

Figure 7. Target object for experimental temperature distribution measurement

Table 3. Parameters used for the temperature distribution simulation

Description	Value	Unit
Heat-transfer coefficient at condensation area h_f	1×10^3, 2×10^3, 3×10^3, 4×10^3, 5×10^3, 6×10^3, 7×10^3, 8×10^3, 9×10^3, 1×10^4, 5×10^4, 1×10^5, 5×10^5, 1×10^6	W/m^{2}K
Diameter of condensation area d_{cd}	0.5, 1, 2, 3, 4, 5, 6	mm
Grid size Δx	2.5×10^{-5}	m
Time step of calculation Δt	5.0×10^{-4}	s
Amount of steps of a calculation	4.0×10^4	-
Amount of grids	362×1,161	-
Element count	420,282	-

The calculation method of simulation was a two-dimensional explicit method with parameters listed in Table 3. If the temperature at position (i, j) and at time t was defined as $\theta_{i,j,t}$,the temperature at the next time step $t+\Delta t$, could be calculated by solving the heat conduction equation in a two-dimensional cylindrical coordinate system Equation (8).

$$\theta_{i,j,t+\Delta t}=\theta_{i,j,t}+\frac{\lambda_{\text{solid}}\rho_{\text{solid}}}{c_p}\cdot\frac{\Delta t}{(\Delta r)^2}\cdot\left(\theta_{i-1,j,t}+\theta_{i,j-1,t}+\theta_{i+1,j,t}+\theta_{i,j+1,t}-4\theta_{i,j,t}+\frac{\theta_{i+1,j,t}+\theta_{i-1,j,t}}{2i}\right) \quad (8)$$

After each step of the calculation, temperature change by surface heat transfer was calculated by Eq. (9) under local thermodynamic equilibrium. θ_f is the temperature of the fluid, and h_f is the heat-transfer coefficient between the fluid and the grid at the surface.

$$\theta_{i,0,t}=\frac{\Delta z\left(h\theta_f+\Lambda_i^-\theta_{i-1,0,t}+\Lambda_i^+\theta_{i-1,0,t}\right)+\lambda_{\text{solid}}\theta_{i-1,0,t}}{\Delta z\left(h+\Lambda_i^-+\Lambda_i^+\right)+\lambda_{\text{solid}}} \quad (9)$$

where

$$\Lambda_i^-=\frac{\lambda_{\text{solid}}+\lambda_{\text{fluid}}}{2}\cdot\left(r_i\ln\frac{r_i}{r_{i-1}}\right)^{-1},\quad \Lambda_i^+=\frac{\lambda_{\text{solid}}+\lambda_{\text{fluid}}}{2}\cdot\left(r_i\ln\frac{r_{i+1}}{r_i}\right)^{-1} \quad (10)$$

Using these equations and parameters, the temperature change of the object was simulated with 15 heat-transfer coefficients at the condensation area, which had seven diameters. Consequently, 105 condensation conditions were simulated.

Each of 36 measurement results were compared with 105 simulation results using the differential time Δt for a temperature increase of 5 ºC between the No. 1 thermistor and the others.

2.3 Histological Comparison

Coagulation mechanism caused by an exposure to the steam-jet were studied through histological comparisons with tissues coagulated with a conventional device. We choose the bipolar electrodes as a device to compare with since the bipolar electrodes have been commonly used and studied. Although it is difficult to determine general settings of the device, we set two work representative settings as shown in Table 4. The one was 3 seconds application with 50W and Effect5 for firm coagulation. Another was 5 seconds application with 20W, the same effect, and a saline irrigation. The saline irrigation is a

technique that a surgeon drops saline on the tip of the bipolar electrodes so as to cool the tip and avoid excessive damage for tissues caused by overheating and desiccation.

Table 4. Coagulation devices and their settings for the histological comparison

General name	Product name	Settings
Bipolar electrode	ERBE VIO®300	Effect5, 50W, 3s
		Effect5, 20W, 5s, saline irrigation
Steam Jet Coagulator	-	50kPa(G), 0.5mm distance, 3s

We coagulated fresh porcine livers for food with these devices and settings. The coagulated parts were cut from a liver and made into tissue blocks. The liver blocks were fixed with 10% neutral buffered formalin fixative, embedded in paraffin, and sliced. The tissue preparations of the slices were made after HE (Hematoxylin-Eosin) dyeing.

2.4 In-vivo Proof-of-Concept

In the preliminary report, the coagulation ability of the steam jet was evaluated using a chicken liver, and successful coagulation under a laparoscopic environment with clear vision was confirmed [7]. In this paper, the authors report experiments for validating two characteristics of the steam-jet coagulation method: faster coagulation without carbonization, and bleeding surface cauterization.

These effects were evaluated experimentally using a porcine subject. Laparotomy was emulated so as to observe the effect directly. A 4-week-old pathogen-free pig under general anesthesia was used to emulate a surgical environment. The experiment was supervised and formally approved by the ethical commission of the Institute of Biomaterials and Bioengineering, Tokyo Medical and Dental University.

The pressure of the steam jet was regulated at 50 kPa(G). The diameter of the nozzle was 1 mm. To obtain that H/D is 0.5~1.0, the nozzle tip of SJC was kept away from the target with approximately 0.5 ~ 1.0 mm while applying the steam jet. The distance was not fixed rigorously due to movements of the target.

3 Results

3.1 Estimation of Experimental Heat-Transfer Conditions

Each of 36 measurement results were compared with 105 simulation results using the differential time Δt for a temperature increase of 5 ºC between the No. 1 thermistor and the others. Therefore, the nine differential times are the targets of the comparison. If one of the experimental results matches the phenomenon associated with an experimental condition, the experimental Δt for each thermistor would be the same as theoretically predicted. Hence, R^2 was used to evaluate the closeness of each simulation result to one of the experimental results. The parameters of the simulation result with the least R^2 of the average of nine differential times were assumed to be the parameters of heat transfer at the surface under the experimental condition. Table 5 shows the estimated heat-transfer coefficient and condensation diameter for each experimental condition. The parameters of the experimental conditions were organized into two terms: P_{st} and H/D, both dimensionless parameters derived by scale. Under the measurement conditions, “N/A” was applied if there was no comparison result with an R^2 of 0.85 or

more. In addition, the measurement was said to have failed if too many drains were shown. Conditions that performed ideal steam condensation heating.

Table 5. Results of matching between experimental temperature distributions and thermal simulations.

H/D	P_{st} =10kPa(G)	30kPa(G)	50kPa(G)	70kPa(G)
0.5	**(>5×10^5, 4), R^2=0.903**	**(>5×10^5, 4), R^2=0.938**	**(>5×10^5, 3), R^2=0.899**	(9×10^3, 3), R^2=0.972
1	**(>5×10^5, 5), R^2=0.881**	(1×10^5, 3), R^2=0.876	(9×10^3, 3), R^2=0.919	(7×10^3, 3), R^2=0.890
	(>5×10^5, 6), R^2=0.921	(5×10^4, 4), R^2=0.868	(1×10^4, 3), R^2=0.861	(1×10^4, 4), R^2=0.902
1.5	(8×10^3, 5), R^2=0.932	N/A	(1×10^4, 5), R^2=0.892	(5×10^3, 5), R^2=0.961
1.67	(too much drain)	(1×10^4, 4), R^2=0.951	(1×10^3, 4), R^2=0.902	N/A
2	(3×10^3, 6), R^2=0.975	(5×10^4, 4), R^2=0.901	(4×10^3, 4), R^2=0.965	(3×10^3, 3), R^2=0.918
3	(1×10^4, 6), R^2=0.862	(6×10^3, 5), R^2=0.882	(2×10^3, 5), R^2=0.945	(1×10^3, 6), R^2=0.897
3.33	(too much drain)	N/A	N/A	N/A
5	(too much drain)	N/A	N/A	N/A

3.2 Histological Comparison

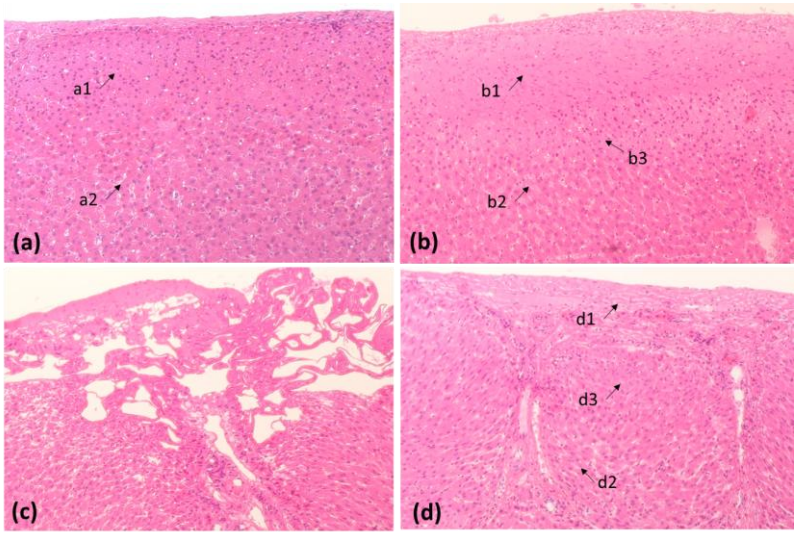

Figure 6. Histological comparison on *ex vivo* porcine liver (HE stain, x100). (a) Control (b) Coagulated with steam-jet (c) Coagulated with bipolar electrode (d) Coagulated with bipolar electrode under saline-irrigation

Figure 6 shows histological images of porcine liver samples. Figure 6 (b), (c), and (d) are the center parts of coagulated liver with the steam-jet, with the bipolar electrodes without saline irrigation, and with the bipolar with saline irrigation, respectively. These specimens were coagulated from the top of the images. The coagulated tissue with steam-jet (b1) is denser than the control (a1). Less sinusoids are observed in b1 than a1. The deeper area (a2, b2) has similar appearance, and thus we assume that no thermal damage appeared at b2. Deformations of hepatic cells and shrinkage of sinusoids are observed at the boundary area (b3). The tissue coagulated with bipolar electrode without saline irrigation (Figure6 (c)) is fractured notably. The image of the coagulated part with bipolar electrodes under saline irrigation (Figure6 (d)) shows different forms of denaturation of hepatic cells. The nucleuses are disappeared at d1 while not at b1. The hepatic cells in the deeper area (d2) have different shapes from the ones at a2. In the boundary (d3), sinusoids are than the control and nucleuses disappeared.

3.3 In-vivo Proof-of-Concept

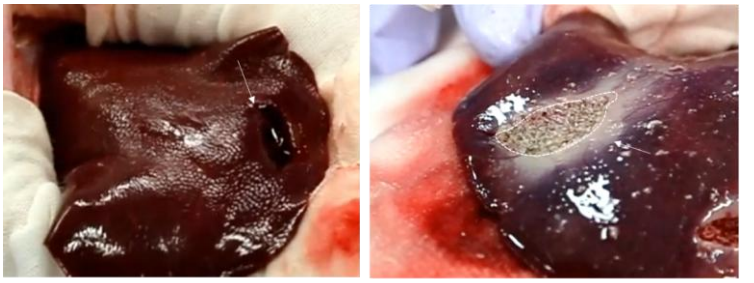

Figure 7. Cauterization experiment on a liver of porcine.

To evaluate SJC's performance on a bleeding surface, bleeding liver parenchyma was selected as the object. The experimental apparatus and result are shown in Figure 7. The surface part of a porcine liver parenchyma was resected by scissors. The resected part was approximately 3 mm deep and 15 mm long. Surface bleeding in the resected area was observed. Blood was not removed before exposure to the steam jet. Cauterization was successfully performed by 30 s application of the steam jet. However, there was collateral thermal damage around the target area.

4 Discussion

The objective of this study was development of a surgical energy device that can perform coagulation for better surgical performances. In the preliminary study, a new type of surgical energy device using a steam jet for faster cauterization without adherence of tissues was proposed. In this study, the authors describe basic principles and cauterization mechanisms of the steam-jet coagulator (SJC) that was newly developed with dry-steam generator for effective heat-transfer with steam.

The conditions with larger values of h that were sufficiently large (h>5.0×10^5 W/m^2) to assume that an ideal condensation heat transfer occurred were indicated in Table 5 as bold characters. Based on the results, the authors confirmed that the SJC was able to perform cauterization and coagulation with indicated design parameters. However, the confirmation was not comprehensive for understanding whole picture of the relationship between the design parameters of the SJC and the successful hemostasis. Further studies with more numbers of trials, and with comparisons to conventional devices are required. However, preparation of equally-controlled bleeding subjects to be coagulated are rather difficult in general. Therefore, well-designed and comprehensive studies are required to describe the differences between the SJC and the conventional devices.

The histological comparison revealed that steam-jet coagulation has unique characteristics. The coagulated hepatic cells by steam-jet were denser than the ones coagulated with the bipolar electrocautery device. The SJC sealed sinusoids in the liver well, and thus successful cauterizations without leakage of blood or bile can be expected. The results obtained in this study are limited because the specimens used were *ex-vivo* samples without perfusions of blood and bile.

Although the collateral thermal damage was observed at the surface, cauterization on the porcine liver parenchyma was successfully performed as shown in Figure 7. The damage was undesirable, and thus there should be further study how to cope with the damage. Moreover, this study evaluated acute

damages and effects. The follow-up observations to study the healing process of the coagulated tissues are required to describe the risks and benefits of the SJC.

Table 5. Various surgical energy devices and their mechanisms [1, 9-12]

Energy type		Effect and mechanism
High Frequency Electricity (0.3~5MHz)	HF	**Cut;** A tissue is ablated and evaporates by consecutive, concentrated HF currents. **Coagulation (ablation);** A tissue is heated gradually by intermittent HF current. **Blend;** Larger duty cycle of HF than coagulation mode enables hybrid function of both above.
	RF	**Ablation;** Radio frequency (RF) current (350~500kHz) generates Joule heat and inductive heat, then a target tissue is ablated.
	MW	**Ablation;** 2.45GHz Microwave (MW) selectively oscillates H_2O molecular, generates inter-molecular f riction heat, and ablates tissues.
	APC	**Contactless coagulation (ablation);** Discharging through argon gas jet and ablate a tissue without direct contact between an electrode and a tissue.
Ultrasonic oscillation		**Coagulation;** A tissue pinched by a gripper is coagulated by means of friction heat. **Cut;** The consecutive application of friction force and the heat dissects the tissue. **Emulsification;** Soft tissues are selectively emulsified and coagulated by the oscillation.
Laser		**Contactless ablation;** A specific wavelength laser generates heat and selectively ablates the tissue. **Contactless cut;** Momentarily heat evaporates the tissue. **Contactless fracture;** Pulse laser generates shock waves near the calculus to destroy the calculus.
Steam-jet*		**Contactless coagulation;** A tissue is heated with condensation heat of steam without direct contact. The coagulated tissue is denser than the one coagulated by a bipolar device (HF) with the saline irriga tion.

** studied in this paper*

There are conventional surgical energy devices used in surgeries. Table 5 is the comparison of the effects and mechanisms between some devices using a high-frequency electricity, an ultrasonic oscillation, a laser, and a steam-jet we studied. The argon plasma coagulator (APC) can perform contactless coagulation using sparks in a jet of argon. The jet flows from the tip of the device and impinges body tissues. Although the APC has several advantages[12], the impinging argon jet sometimes causes fatal or unfatal gas embolism when the gas is injected into open veins which is exist at bleeding point[13]. By contrast, steam-jet will not cause the gas embolism due to steam's condensation. Moreover, the histological image of coagulated liver with steam-jet showed any evidence of invasion of steam into the liver tissue. Another conventional contactless device is the surgical laser device which can perform ablating, cutting, and fracturing the tissues. Since the laser devices are not used for cauterization, the use case of the device will be different from the one of the SJC. The unique characteristics and some advantages are described through the comparisons based on outcomes of this study.

5 Conclusion

Basic principles and cauterization mechanisms of cauterization method with steam-jet were studied. The steam-jet coagulator (SJC) was newly developed with dry-steam generator for effective heat-transfer with steam. The condensation heat-transfer coefficient at the surface was estimated through theoretical simulation and experimental temperature distributions inside the heated object by impinging steam-jet. Histological comparison of coagulated hepatic tissues revealed that steam-jet can coagulate tissue denser and can seal sinusoids better than the ones coagulated with the bipolar electrocautery device even if the saline irrigation method was used. Successful coagulation and cauterization were performed on the *in-vivo* experiment using porcine liver, and thus the feasibility of the proposed method was confirmed. Further developments and studies on this unique device

ACKNOWLEDGMENT

This work was supported by the Grant-in-Aid for Scientific Research (KAKEN) (B) No. 16H04295 from JSPS (Japan Society for the Promotion of Science). I would like to thank Naofumi Tanaka, MD, Kazuyuki Kojima, MD, and Taro Sugimoto, MD in Tokyo Medical and Dental University for kind advices for the developing of the device as surgical experts.

REFERENCES

[1]. Feldman, L.S., et al., *The SAGES Manual on the Fundamental Use of Surgical Energy (FUSE)*. 2012, New York: Springer-Verlag (United States).

[2]. Rassweiler, J., et al. *The past, present and future of minimally invasive therapy in urology: a review and speculative outlook*. Minimally Invasive Therapy & Allied Technologies, 2013. 22(4): p. 200-209.

[3]. Lang, B.H., et al., *A Systematic Review and Meta-analysis Comparing the Efficacy and Surgical Outcomes of Total Thyroidectomy Between Harmonic Scalpel Versus Ligasure*. Annuals of Surgical Oncology, 2013. 20(6): p. 1918-1926.

[4]. Lorenzo, N.D., et al., *Radiofrequency versus ultrasonic energy in laparoscopic colorectal surgery: a metaanalysis of operative time and blood loss*. Surgical Endoscopy, 2012. 26(10): p.2917-2924.

[5]. Wu, M.P., et al., *Complications and recommended practices for electrosurgery in laparoscopy.* The American Journal of Surgery, 2000. 179 (1): p. 67-73.

[6]. Milsom, J.W., et al., *Laparoscopic Colorectal Surgery*, 2nd edition ed2006, New York: Springer-Verlag (United States).

[7]. Yoshiki, H., et al., *Surgical Energy Device using Steam Jet for Robotic Assisted Surgery*. Proceedings of 37th Annual International Conference of the IEEE Engineering in Medicine and Biology Society (EMBC), Milan, Italy, 2015. p. 6872-6875.

[8]. Wagner W., et al., *The IAPWS Formulation 1995 for the Thermodynamic Properties of Ordinary Water Substance for General and Scientific Use*, Journal of Physical and Chemical Reference Data, 2002. 31(2): p. 387-535.

[9]. Hay D.J., *Electrosurgery*, Surgery, 2007. 26(2): p. 66-69.

[10]. Denys A.L., et al., *Radio-frequency tissue ablation of the liver: in vivo and ex vivo experiments with four different systems*. European Radiology, 2003. 13(10): p. 2346-2352.

[11]. Boutros C., et al., *Microwave coagulation therapy for hepatic tumors: Review of the literature and critical analysis*. Surgical Oncology, 2010. 19(1): e22-e32.

[12]. Raiser J., et al., *Argon plasma coagulation for open surgical and endoscopic applications: state of the art*. Journal of Physics D: Applied Physics, 2006. 39: p. 3520-3523.

[13]. Sankaranarayanan, G., et al., *Common uses and cited complications of energy in surgery*, Surgical Endoscopy, 2013. 27(9): p. 3056-3072.

